Mechanism of Interaction between the General Anesthetic Halothane and a Model Ion Channel Protein, III: Molecular Dynamics Simulation Incorporating a Cyanophenylalanine Spectroscopic Probe

Hongling Zou, Jing Liu, and J. Kent Blasie*
Department of Chemistry, University of Pennsylvania, Philadelphia, Pennsylvania

ABSTRACT A nitrile-derived amino acid, Phe_{CN}, has been used as an internal spectroscopic probe to study the binding of an inhalational anesthetic to a model membrane protein. The infrared spectra from experiment showed a blue-shift of the nitrile vibrational frequency in the presence of the anesthetic halothane. To interpret the infrared results and explore the nature of the interaction between halothane and the model protein, all-atom molecular dynamics (MD) simulations have been used to probe the structural and dynamic properties of the protein in the presence and absence of one halothane molecule. The frequency shift analyzed from MD simulations agrees well with the experimental infrared results. Decomposition of the forces acting on the nitrile probes demonstrates an indirect impact on the probes from halothane, namely a change of the protein's electrostatic local environment around the probes induced by halothane. Although the halothane remains localized within the designed hydrophobic binding cavity, it undergoes a significant amount of translational and rotational motion, modulated by the interaction of the trifluorine end of halothane with backbone hydrogens of the residues forming the cavity. This dominant interaction between halothane and backbone hydrogens outweighs the direct interaction between halothane and the nitrile groups, making it a good "spectator" probe of the halothane-protein interaction. These MD simulations provide insight into action of anesthetic molecules on the model membrane protein, and also support the further development of nitrile-labeled amino acids as spectroscopic probes within the designed binding cavity.

INTRODUCTION

Recent investigations of ion channels in the central nervous system (1,2) have led to the belief that inhaled general anesthetic molecules interact directly with the hydrophobic cavities within and/or on the surface of these membrane proteins, thereby modulating their activity. However, exactly how this is achieved remains a mystery, because little is known about the generally weak interaction between anesthetics and their presumed protein targets at the atomic level.

To investigate the structural features of potential anesthetic binding sites and the nature of the interaction between anesthetic molecules and these sites in membrane proteins, simplified model membrane proteins with designed cavities have been developed (3,4). For example, in part I under this title (5), a new halothane-binding model membrane protein (hbAP1) was studied. By comparison with an otherwise identical control protein lacking only the designed cavity, we demonstrated via x-ray reflectivity that the amphiphilic 4-helix bundle hbAP1 was able to bind halothane with the halothane localized to the neighborhood of the designed cavity at lower concentrations of halothane. This simplified synthetic model membrane protein allows for the easy mutation of residues forming the binding site and utilization of sophisticated physical-chemical techniques to investigate the halothane-protein interaction in detail.

Spectroscopic probes have been introduced close to ligand-binding sites in proteins to monitor both the ligand binding and its effect on protein conformation. For example, the fluorophore tryptophan has been frequently used to study the association of volatile anesthetics, including halothane, with the designed binding sites in both water-soluble and membrane-protein models (3,6). However, the quenching of fluorophore emission by the anesthetics can be simply collisional, thereby not necessarily reflecting the existence of a distinct binding site. Moreover, the indole ring of tryptophan is suspected to have a direct interaction with halothane (6,7), increasing the complexity of detecting the binding of halothane within the hydrophobic cavities.

Infrared spectroscopic probes, such as the nitrile group, can serve as effective internal probes of the local protein environment upon ligand binding or folding in biological proteins (8,9). Having a small size and intermediate polarity, the nitrile group is expected to minimally perturb its environment within a protein. In part II under this title (10), we describe the use of a nitrile-labeled amino acid, Phe_{CN}, as an infrared probe to study halothane binding to a model membrane protein. Placing the label Phe_{CN} adjacent to the designed cavity in hbAP1 provides the advantage of using both fluorescence and infrared spectroscopic techniques simultaneously. The infrared results showed that the nitrile stretching vibrational frequency experienced a blue-shift upon binding halothane. Due to the intrinsic sensitivity of the nitrile stretching vibration, the observed nitrile vibrational frequency shift may be caused by many factors, ranging from a direct interaction of halothane with the probe to an indirect effect due to a halothane-induced change in the probe's local protein and/or solvent environment. In other

Submitted August 13, 2008, and accepted for publication January 28, 2009.

*Correspondence: Ujkblasie@sas.upenn.edu or jkblasie@sas.upenn.edu

Editor: Thomas J. McIntosh.

0006-3495/09/05/4188/12 $2.00

doi: 10.1016/j.bpj.2009.01.054

words, a direct interpretation of the frequency shift may be inaccessible from the experimental studies alone. The use of molecular dynamics (MD) simulation to probe the structural and dynamic properties of membrane proteins is by now well established (11–14). Given the interaction potentials commonly used in such simulations of solvated protein systems, they provide not only the possibility of determining the origin of the vibrational spectral shift, but if successful, they can then also provide a detailed description of the motions of the anesthetic molecule within the binding site and the interactions between the anesthetic molecule and the model membrane protein at the atomic level.

In this work, we performed classical MD simulations to study halothane binding to the designed hydrophobic cavity within the core of the hydrophilic domain of the amphiphilic 4-helix bundle peptide hbAP1-Phe$_{CN}$. The effect of Phe$_{CN}$ substitution on the peptide bundle's structure was inspected. Halothane's motion within the hydrophobic cavity was analyzed to show the retention of localization of halothane in the cavity. We calculated the vibrational frequency shift of the nitrile groups for each of the four Phe$_{CN}$ residues within the peptide bundle, averaged over the four less-than-equivalent residues and over time, to provide an explanation of the experimentally observed blue-shift. The agreement achieved between MD simulation and experimental results added credibility to the further findings provided by simulations. These revealed how the anesthetic molecule interacts with peptide bundle and affects bundle dynamics on the timescale of nanoseconds. In addition, the direct interaction between halothane and infrared probe nitrile groups was excluded, thereby supporting the potential for the direct nitrile labeling of residues forming the anesthetic binding sites in such model proteins in future studies.

Simulation systems and methodology

The hbAP1 peptide (5) was derived from hbAP0 (3,4) by mutating Ala^{8} to Leu^{8} to consider only one binding cavity at Ala^{19}, and mutating Leu^{22} to Met^{22} to allow future labeling experiments with Se-Methionine. Mutation of Trp^{15} to a nonbiological amino acid Phe$_{CN}^{15}$ (i.e., Hζ on phenyl ring of Phe was replaced by C = N, as shown in Fig. 1) was made to introduce nitrile groups adjacent to the designed halothane binding cavity as an infrared probe as well as a fluorophore with a high quantum yield (10). We designate this peptide as hbAP1-Phe$_{CN}$. Both hbAP1 and hbAP1-Phe$_{CN}$ peptide were initially constructed as ideal right-handed α-helices using INSIGHTII (Accelrys Software). The four-α-helix bundle was formed by associating two dihelices in *syn* topology, each dihelix linked by a disulfide bond, with the nonpolar side chains in the hydrophilic domain and polar side chains in the hydrophobic domain placed within the core of the four-α-helix structure.

A solvent environment was generated by inserting the 4-helix bundle peptide into preequilibrated water-octane slabs with the interface between the hydrophilic and hydrophobic domains of the bundle aligned with that between the slabs, and any overlapping solvent molecules were removed. The dimensions (50 × 50 × 145 Å^3) of the MD cell were chosen to be large enough to ensure isolation of both the amphiphilic 4-helix bundle and the interface while using periodic boundary conditions to model an intrinsically two-dimensional monolayer system in the simulations. This requirement remained valid throughout the entire simulation.

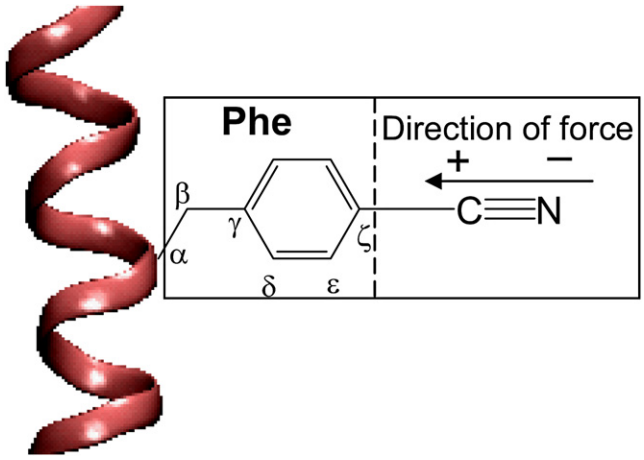

FIGURE 1 Illustration of the chemical structure of nonbiological amino acid Phe$_{CN}$ and the definition of the nitrile bond axis. The helix to which the Phe$_{CN}$ residue is attached is shown in ribbon representation.

The system was first minimized for 2000 steps to eliminate the tension between different components. The minimized system was then gradually heated over 100 ps to a final temperature of 300 K. Finally dynamics trajectories were generated for the simulation systems under constant NPT conditions with the structures saved every 0.5 ps.

All the simulations were carried out using the NAMD2 package (15), which incorporates features such as periodic boundary conditions and the particle mesh Ewald method for full evaluation of electrostatic interactions. Nonbonded interactions were calculated with a cutoff distance of 12 Å and a switching function was used to relax the van der Waals potential to zero over a distance of 2 Å. Constant temperature was controlled by Langevin dynamics and the pressure was maintained at 1 atm using the Nose-Hoover Langevin Piston method. The SHAKE algorithm was used to constrain all bonds between hydrogens and heavy atoms with a tolerance of 10^{-8} Å. An integration time step of 1 fs was used for bonded and nonbonded interactions, and full electrostatic forces were evaluated every other time step.

CHARMM22 all atom force field (16) was used to describe the protein interactions, and the TIP3P model (17) was used for water molecules. The parameters used for octane molecules were those recommended by MacKerell et al. (16) for methyl and methylene groups. The nitrile of Phe$_{CN}$ was modeled by analogy to the nitrile in 3-cyanopydine, implemented in CHARMM31 force field (18).

Simulation on hbAP1-Phe$_{CN}$ at octane-water interface (apo bundle, with halothane absent) was performed for 5 ns. After the apo peptide bundle reached equilibrium, anesthetic molecule was introduced into the stable four-helix bundle hbAP1-Phe$_{CN}$. Two parallel simulations on holo-system (bundle with halothane present) were run for 1 ns starting from such ''preequilibrated'' conditions, with each of them chosen from slightly different initial configurations of peptide bundle from the same preequilibrated apo system. Most results were shown based on the first parallel simulation (simulation I) if not otherwise specified; some results from the second parallel simulation (simulation II) were also presented to show the similarity of the results from parallel simulations. In these parallel simulations, halothane was constructed using INSIGHTII program. A single halothane molecule was placed within the hydrophobic core of the bundle with its center of mass aligned with those of the four Ala^{19} residues. The halothane was oriented as the carbon-carbon axis parallel to the long axis of the peptide bundle, with the dihalogenated carbon atom facing down to the Phe$_{CN}$ residues. The parameter set derived from ab initio calculation (19) was used for the halothane molecule.

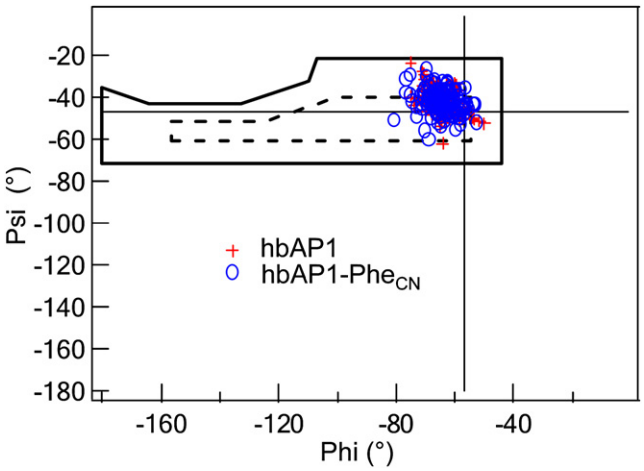

FIGURE 2 Ramachandran plot for residues 2–36 in all the helices of the apo protein hbAP1 (*cross*) and its mutant hbAP1-Phe$_{CN}$ (*circle*) at the water-octane interface. The backbone conformation angles phi and psi are calculated as averages over the last 1 ns of the simulation. The dashed perimeter corresponds to the most favorable combinations of phi/psi values for a right-handed α-helical conformation, and the solid perimeter highlights the somewhat larger ''Ramachandran-allowed'' region.

RESULTS AND DISCUSSION

Overall structure of the apo peptide and effects of Trp → Phe$_{CN}$ mutation

Within 5 ns of simulation, the de novo designed amphiphilic hbAP1 peptide, initially built from straight uncoiled α-helices, spontaneously evolves to a stable coiled-coil four-helix bundle structure at the water-octane interface, which agrees with grazing incidence x-ray diffraction measurements (in parts I (5) and II (10) under this same title). Characterization of the hbAP1-Phe$_{CN}$ peptide suggests the same structural evolution as with the hbAP1 peptide. These structural properties are analogous to those for the amphiphilic AP0 peptide studied elsewhere (20), which was developed using the same sequence design strategy as for hbAP1 in terms of the amphiphilicity of the bundle, albeit for entirely different applications. Details of these characterizations are similar to those described for the simulation of the AP0 peptide (20).

Two structural features are examined here to demonstrate that Trp → Phe$_{CN}$ mutation perturbs neither the secondary structure nor the quaternary structure of the peptide bundle. The secondary structure of hbAP1 and its mutant hbAP1-Phe$_{CN}$ are characterized by Ramachandran plots of the time-averaged backbone phi/psi angle pairs of all residues, except the N-terminal capping residues and C-terminal Gly linker residues (Fig. 2). The majority of residues of both peptides remain within the allowed region for an α-helical conformation over the entire trajectory. Most of the phi/psi pairs of hbAP1-Phe$_{CN}$ overlap with those of hbAP1. The time-averaged interhelix separation between neighboring dihelices for each heptad is calculated for hbAP1 and its mutant hbAP1-Phe$_{CN}$ to characterize the quaternary structure of the peptide bundle (see Fig. S1 in the Supporting Material). No apparent difference is observed at the mutation site (residue number 15) as well as other parts of helices. The above structural analyses indicate a minimal perturbation on the structure of the peptide bundle by introducing a nonbiological amino acid Phe$_{CN}$ adjacent to the designed hydrophobic cavity of the protein. We also note that the mutation of Trp → Phe$_{CN}$ has no measurable effect on the halothane binding affinity (10). It is therefore reasonable to relate the results from the x-ray reflectivity experiments for hbAP1 (5) to the infrared spectroscopic studies of the nitrile labeled hbAP1 peptide (10) and further compare those results with these MD simulations.

Localization of the halothane at the designed cavity

X-ray reflectivity experiments demonstrated that at lower anesthetic concentrations of 3–4 molecules per bundle, the halothane was localized along the length of the bundle within a symmetric unimodal distribution centered on the position of the designed binding cavity, which was lined with Ala^{19} residues in the core of the peptide bundle's hydrophilic domain (5). In the simulation, the halothane was therefore initially placed at the center of the designed binding cavity, which was defined as the centroid of the four Ala^{19} residues. Halothane was originally oriented with the carbon-carbon axis parallel to the long axis of the peptide bundle, with the dihalogenated carbon facing toward the Phe$_{CN}$ residues. During the simulation trajectory, halothane remains within the core of the cavity on the nanosecond timescale. However, it nevertheless exhibits a significant amount of translational

and rotational motion (Fig. 3). The halothane occupies different positions along the long axis of the peptide bundle within the cavity, with a fluctuation of ± 2 Å centered about the Ala^{19} residues. In the process, halothane correspondingly samples several discrete orientations with respect to the long axis of the peptide bundle, with each orientation persisting from tens to hundreds of ps. However, there is no single strongly preferred orientation of halothane toward any specific residues. This same behavior of halothane was also observed in a parallel simulation. These results agree qualitatively with experimental measurements at lower halothane concentrations, but greater than one halothane per bundle. The translational dynamics along the bundle axis, even for a single halothane molecule, agree with the x-ray reflectivity results where halothane was found to be localized along the length of the bundle to the neighborhood about the designed cavity (5) at 3–4 halothanes/bundle. The coupled translational and rotational dynamics of halothane within the cavity suggest a collisional mechnism for the quenching of the adjacent fluorophores' emission by halothane at 1–10 halothanes/bundle (10). We did not observe a larger extent of halothane translational diffusion along the core of the bundle as the x-ray reflectivity experiment suggested. This likely arises from the somewhat larger number of halothane molecules/bundle, achieved as a lower limit in the x-ray reflectivity experiments to date, as well as the very limited duration of the simulation trajectory in comparison to the experiment.

Interpretation of infrared spectroscopy

The infrared experiments on hbAP1-Phe_{CN} exhibited a blue-shift of the nitrile stretching vibration frequency when halothane was introduced into the system.

Infrared spectra of the nitrile vibration measure a statistically averaged absorption of all Phe_{CN} residues within the system. There are four Phe_{CN} residues adjacent to the cavity within the peptide bundle, and although they occupy the same position in the sequence of each helix, they become inequivalent in the 4-helix bundle, each of them with a different conformation in a different environment that varies with time. In addition, a large ensemble of peptide bundles could sample these conformations at any particular time. This averaging phenomenon renders the environment of the Phe_{CN} oscillators in the bundle ensemble rather complex. MD simulation provides a minimal approach to address this issue, averaging over the simulation trajectory for a single amphiphilic 4-helix bundle in an explicit interfacial solvent environment to sample the different conformations accessible to the peptide; it is also necessary to decompose the infrared spectra by analyzing the frequency shift for individual oscillators.

Analysis of nitrile vibrational motion in terms of different force components exerted on nitriles

A shift in the vibrational frequency of a particular group (e.g., diatomic for the nitrile group) within a macromolecule can arise from a change in bonding and/or nonbonding interactions. The latter exert forces on the atoms within the group arising from other atoms in their local environment, including those of the macromolecule itself as well as those of its solvent, the relevant component being that directed along the corresponding bond(s) (21,22). For the nitrile oscillator in the Phe_{CN} residue, which is covalently linked through the phenyl ring to the peptide backbone, the total force exerted along the nitrile triple bond can be approximated as that exerted on the N atom directed along the bond axis, because the C atom is attached to a substantially larger mass comprised of the remainder of the residue (Fig. 1). When the local environment of the nitrile oscillator in the Phe_{CN} residue exerts a repulsive force on the nitrogen atom compressing the nitrile triple bond, the nitrile stretching vibration will be shifted to higher frequency, whereas an attractive force on the nitrogen stretching the bond would result in a shift to lower frequency.

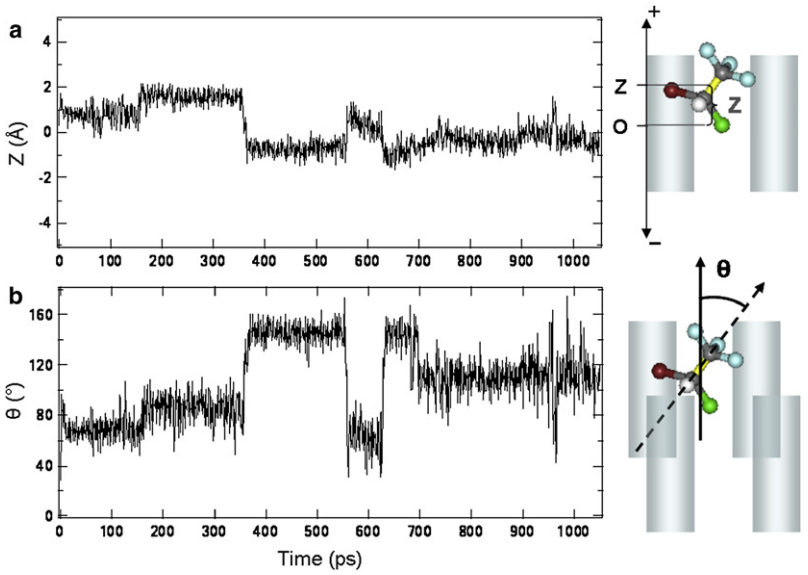

FIGURE 3 Time evolution of the halothane's translational (*a*) and rotational (*b*) motion within the hbAP1-Phe_{CN} bundle. The halothane's translational displacement *Z* is defined as the distance from the center of the halothane molecule (*Z*) to the center of the four Ala^{19} residues (*O*) projected along the peptide bundle long axis. The halothane's rotational angle θ is defined as the angle between the *C-C* axis of the halothane molecule and the peptide bundle long axis.

We have computed the contributions from different nonbonding forces, i.e., electrostatic and van der Waals, exerted on the nitrogen of each Phe_{CN} residue projected along its nitrile bond and averaged over the simulation trajectory for both the apo and holo hbAP1-Phe_{CN} (i.e., in the absence and presence of halothane, respectively). The results are summarized in Table 1. As indicated in the table, the electrostatic force dominates the total force. Upon adding the halothane into the cavity, the change of electrostatic force is threefold larger than the change of van der Waals force, accounting for ~70% of the change of total force in most cases. For Phe_{CN}^{55} and Phe_{CN}^{95}, the two residues that are buried inside the nonpolar core of the bundle, with their C_N bond pointing toward the interior, the dominant role of the electrostatic force is more significant than the cases for Phe_{CN}^{15} and Phe_{CN}^{135} residues that have their C = N bond pointing toward the exterior of the bundle, partially accessible to solvent (Fig. 4). Introducing halothane into the system perturbs the local electrostatic field, especially influential to the region close to the designed hydrophobic cavity. We also notice from the table that the fluctuations in the van der Waals forces are greater than those of the electrostatic forces, relative to their respective mean values, the fluctuations for both being larger than the changes in these component forces arising from the introduction of halothane into the cavity within the core of the bundle. This demonstrates that the packing of side chains forming the cavity is highly dynamic and flexible. This dynamic feature will be further elaborated in the next subsection.

Prediction and interpretation of the blue shift

The dominant role of electrostatic forces in the halothane-induced shift of the Phe_{CN} nitrile group's vibrational frequency allows us to analyze the infrared results in terms of the vibrational Stark effect. Enlightened by Sunydam's estimate of changes in the electric field within a protein from the frequency shift of a calibrated aromatic nitrile vibration (23), we then estimated the frequency shift for each Phe_{CN} nitrile vibration from the corresponding electrostatic force exerted on its nitrogen along the nitrile bond axis. The observed vibrational frequency shift $\Delta\nu_{obs}$ in response to the change of the electric field $\Delta\vec{E}$ through a calibrated vibrational probe is

$$\Delta\nu_{obs} = -\Delta\vec{\mu}_{probe} \times \Delta\vec{E} = -\Delta\vec{\mu}_{probe} \times \Delta E_{//}. \quad (1)$$

$\Delta\vec{\mu}_{probe}$ is the transition dipole moment of the vibrational probe. $\Delta E_{//}$ is the change in electric field projected on the direction of $\Delta\vec{\mu}_{probe}$, which lies along the nitrile bond axis in mononitriles (24,25). Defining the nitrile bond axis as pointing from the nitrogen toward the carbon, substituting the $\Delta\vec{\mu}_{probe}$ of an aromatic nitrile analog from its Stark spectrum (23), leads to:

$$\begin{aligned}\Delta\nu_{obs} &= -0.69\left(cm^{-1}/(MV/cm)\right) \times \Delta E_{//} \\ &= -0.69\left(cm^{-1}/(MV/cm)\right) \times \Delta F_{//}/q. \end{aligned} \quad (2)$$

$\Delta F_{//}$ is the change of force exerted on nitrogen along the nitrile bond axis between the holo- and the apo form of hbAP1-Phe_{CN} ($F_{//,holo}$-$F_{//,apo}$), in the unit of kcal/mol·Å. The partial charge q on the nitrogen atom of Phe_{CN} in the simulation is −0.53e. Equation 2 can be converted to Eq. 3 (refer to Note S1 in the Supporting Material for details):

$$\Delta\nu_{obs} = 5.65\left(cm\text{-}^{1}/(Kcal/mol\ Å)\right) \times \Delta F_{//}. \quad (3)$$

According to this calibration, the presence of halothane in the cavity that causes a change in force of 1 Kcal/mol·Å

TABLE 1 Total forces exerted on the nitrile nitrogens of the Phe_{CN} residues projected along C = N axis, averaged over the whole MD trajectory

		VDW	Electrostatics
Phe_{CN}^{15}	$F_{//.apo}$	1.88 ± 3.06	−4.69 ± 1.88
	$F_{//.holo}$	1.52 ± 2.67	−3.77 ± 1.14
	$F_{//.holo}$-$F_{//.apo}$	−0.36	+0.92
Phe_{CN}^{55}	$F_{//.apo}$	2.70 ± 4.34	−5.08 ± 2.11
	$F_{//.holo}$	2.74 ± 3.93	−5.64 ± 1.40
	$F_{//.holo}$-$F_{//.apo}$	+0.04	−0.56
Phe_{CN}^{95}	$F_{//.apo}$	2.48 ± 3.11	−4.72 ± 1.14
	$F_{//.holo}$	2.47 ± 3.32	−3.69 ± 1.14
	$F_{//.holo}$-$F_{//.apo}$	−0.01	+1.03
Phe_{CN}^{135}	$F_{//.apo}$	1.27 ± 3.90	−4.84 ± 2.43
	$F_{//.holo}$	1.69 ± 2.65	−4.05 ± 1.25
	$F_{//.holo}$-$F_{//.apo}$	+0.37	−0.79

Define the nitrile bond axis as pointing from the nitrogen toward the carbon, as shown in Fig. 1, to consider the sign of the force calculation.
The total force includes the electrostatic and van der Waals contributions, with a cutoff distance 12 Å.
For the convenience of calculation, the forces were calculated simply by averaging the values over the whole trajectory, not by fitting Gaussian functions to the histograms of the forces as that in Table 2. Therefore, the values of the total forces may be slightly different from those in Table 2. However, both averaging methods provide the same signs and magnitudes of the corresponding forces.
The values are given in units of kcal/(mol·Å).
The sampling frequency is every 20 ps for a total of 1 ns trajectory.

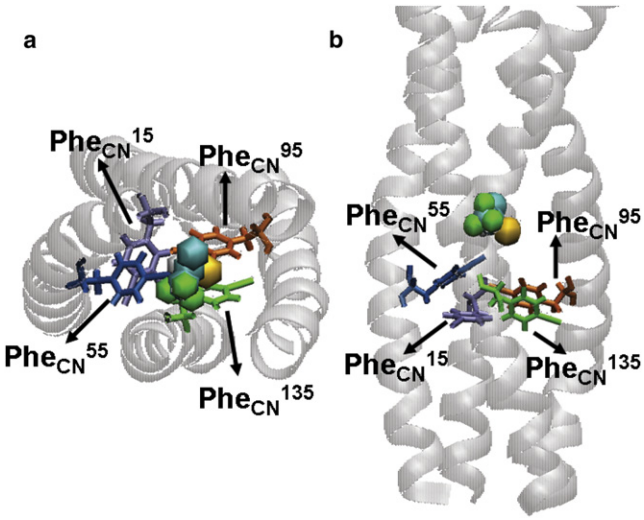

FIGURE 4 Instantaneous configuration of the hbAP1-Phe$_{CN}$ with the halothane binding to the cavity viewed from the top (*a*) and from the side (*b*). The peptide is shown in ribbon representation and the four Phe$_{CN}$ residues in wire-frame representation.

along the nitrile bond axis would render a shift in the C = N stretching frequency of +5.65 cm^{-1}.

We calculated the total force exerted on the nitrogen of individual Phe$_{CN}$ residue projected along the nitrile bond axis for both the apo and holo form of hbAP1-Phe$_{CN}$. The histogram distribution of each force over the simulation trajectory was evaluated and fitted by a Gaussian function to obtain a time-averaged force. The mean and the widths of these forces from the histogram distribution are summarized in Table 2. The frequency shift due to halothane binding estimated from the force change calibrated from Eq. 3 is also summarized in the table. As shown, the estimated nitrile frequency shifts for all four Phe$_{CN}$ residues are mostly positive except for the one having the smallest magnitude. Each nitrile group experiences a different force change, suggesting heterogeneity in the conformational environments for Phe$_{CN}$ residues. The experimentally measured frequency shift in general reflects a superposition of the forces along different nitrile bonds. Thus we obtained an average frequency shift of ~+3 cm^{-1}. The frequency shift due to halothane binding from the force change for a parallel simulation was also estimated with an average frequency shift of ~+6 cm^{-1} (see Table S1 in the Supporting Material). The agreement between simulation and experiment (~+6 cm^{-1}) is considered quite good given that we predict both the correct sign and the approximate magnitude of the frequency shift, the latter to within a factor of 2. (At this point, we consider the correct sign and approximate magnitude of the frequency shift predicted from MD simulation as the most important factors. There are several possibilities to explain the lack of even better agreement with regard to the magnitude. First of all, the concentration of halothane in the simulation is not the same as used in the infrared experiment. In the infrared experiment, a higher concentration of halothane is used (i.e., ~6–7 halothanes/bundle) due to the low sensitivity of the instrument. In our peptide bundle, there are four Phe$_{CN}$ residues at the binding site with heterogeneous environment, the superposition of all of them giving the averaged nitrile vibration spectra. Therefore, in the simulation, we chose one halothane per bundle in the cavity to avoid adding complexity to the already-complicated system. However, we believe that there is only one halothane within the cavity even in the higher concentrations of halothane in

TABLE 2 Time-averaged forces exerted on the nitrile nitrogens of Phe$_{CN}$ residues projected along the C=N axis

		Phe$_{CN}^{15}$		Phe$_{CN}^{55}$		Phe$_{CN}^{95}$		Phe$_{CN}^{135}$	
		MF	SD	MF	SD	MF	SD	MF	SD
Total	$F_{//.apo}$	−3.31	2.72	−3.52	3.00	−2.78	2.79	−4.16	2.04
	$F_{//.holo}$	−2.87	2.43	−3.88	2.80	−2.03	2.30	−2.92	2.19
	$F_{//.holo} - F_{//.apo}$ ($\Delta\nu_{obs}$)	+0.44 (+2.5)		−0.36 (−2.0)		+0.75 (+4.2)		+1.24 (+7.0)	
Protein	$F_{//.apo}$	−1.73	2.28	−3.95	1.66	−2.08	2.51	−5.00	3.20
	$F_{//.holo}$	+0.17	2.49	−4.68	1.53	−1.48	2.18	−4.28	2.46
	$F_{//.holo} - F_{//.apo}$ ($\Delta\nu_{obs}$)	+1.90 (+10.7)		−0.73 (−4.1)		+0.60 (+3.4)		+0.72 (+4.1)	
Solvent	$F_{//.apo}$	−1.48	1.98	+0.35	0.80	−0.93	1.04	1.64	3.54
	$F_{//.holo}$	−3.08	1.16	+0.77	1.20	−0.44	0.60	1.73	1.66
	$F_{//.holo} - F_{//.apo}$ ($\Delta\nu_{obs}$)	−1.60 (−9.0)		+0.42 (+2.3)		+0.49 (+2.7)		+0.09 (0.5)	
Halothane	$F_{//.holo}$	+0.05	0.05	−0.02	2.42	−0.10	0.14	0.00	0.07
	($\Delta\nu_{obs}$)	(+0.3)		(−0.1)		(−0.6)		(0.0)	

The total forces are decomposed into the contributions from the protein, the solvent and the halothane, respectively. The estimated frequency shifts due to halothane binding are also included. In this table, calculation of the time-averaged mean forces is from fitting a Gaussian function to the histogram of the force over the simulation trajectory for each component. Therefore, the values of the total forces are not exactly the same as the summation of the three individual components from the protein, the solvent and the halothane.

Define the nitrile axis as pointing from the nitrogen toward the carbon, as shown in Fig. 1, to consider the sign of the force calculation.

The mean force (MF) F_0 and the standard deviation (SD) σ were obtained by fitting a Gaussian function $A\exp[-(F-F_0)^2/2\sigma^2]$ to the histogram of the force over the simulation trajectory.

Values of forces are given in the units of kcal/(mol·Å).

In the parentheses, frequency shifts due to halothane binding were calibrated from the force changes based on Eq. 3. The values are in the units of cm^{-1}.

Sampling frequency is every 20 ps for a total of 1 ns trajectory.

the experiment, because the nonpolar core is not big enough to accommodate two halothane molecules side by side, the diffusion along the core of the bundle having been shown to be one-dimensional ''single file'' at these higher concentrations (in part II under this same title (10)). Therefore we consider the simulation results to be relevant to the experiment, although the lack of more halothane molecules elsewhere in the bundle could produce better or lesser agreement with regard to the magnitude of frequency shift in the experiment. Secondly, we assume the time-average forces to represent ensemble average forces, the commonly accepted ergodic hypothesis in simulations. However, we acknowledge that the simulations remain limited by the duration of the trajectory. Thirdly, the sequence we use in part II (10) and this work is not completely identical in terms of position of Met. However, we have discussed in the previous context of this work about the effect of mutation to sequence in parts I (5), II (10), and III. This slight difference in sequence does not produce any difference in structure and binding affinity. Considering the size, shape, and polarity of Met and Leu, we do not expect any significant difference in frequency shift for either. Thus, despite this relatively small discrepancy in the magnitude of the spectral shift between simulation and experiment, we believe the overall results remain significant.)

The observed blue-shift of nitrile vibration may be caused by the change of any component comprising the oscillators' environments. The nitrile stretching vibration of the Phe_{CN} residue has been shown to be sensitive to solvent (8,26). Inspection of a systematic sampling of instantaneous configurations for holo hbAP1-Phe_{CN} does reveal that not all Phe_{CN} residues are entirely buried in the nonpolar core of the bundle. However, this is true even for the apo form (i.e., without halothane). To further explore the origin of the force change leading to the blue-shift, we then decompose the total force into contributions from the protein, the solvent and the halothane, respectively. The corresponding results are summarized in Table 2. These show that the force changes from the peptide environment are generally larger than the force changes from the solvent environment, and mainly determine both the sign and the magnitude of Phe_{CN} residues' vibrational frequency shifts. The force change from the solvent environment for each oscillator either possesses the opposite sign to that of the total force change or exerts a smaller effect than that from the protein environment. This is an indication that changes in solvent accessibility of the Phe_{CN} residues cannot account for the observed blue-shift of nitrile vibrational frequency. Halothane itself also exerts only a small component of the total forces directed along the nitrile bond, thereby having only a negligible effect on the frequency shift. This result discounts any strong direct interaction of the halothane with Phe_{CN} nitrile groups. Thus, halothane's impact on the nitrile probes is rather indirect, namely the introduction of halothane into the cavity induces primarily a change in electrostatic protein environment of the four probes inside the bundle adjacent the cavity.

Dynamic nature of the cavity

We again note the dynamic nature of the peptide's internal cavity provided from Table 2, namely the fluctuations in the component forces are comparable or greater than their respective mean forces, both being larger than the changes in the total mean force exerted on the nitril groups arising from halothane binding. The accuracy of the time-averaged total mean force and resulting vibrational frequency shift calculated from the simulation trajectory for a single structure depends on obtaining a structure for the model membrane protein that well represents the ''statistically averaged structure,'' which can be a challenge even if the structure appears to become well equilibrated over the course of the trajectory. The initial choice of configuration has always been a challenging issue. However, it has been observed for a similar amphiphilic 4-helix bundle peptide system that distinct initial configurations can converge with regard to their major structural features (27) given sufficient time. Similarly in this work, the introduction of halothane into an initial configuration for the 4-helix bundle of straight untilted α-helices and into that of a preequilibrated coiled-coil structure developed for the apo form were investigated, and the parallel simulations subsequently analyzed. These two very different initial configurations were found to evolve to similar conformations, both in terms of the protein's secondary and quaternary structure, and exhibiting a cavity of comparable composition and size with the incorporation of halothane, suggesting that a reasonable statistically representative structure has been attained. Therefore, we believe this method can still serve as an important approach to interpret and predict experimental results.

Specific halothane interaction with the designed cavity

The MD simulations predict the experimental results from infrared spectroscopy reasonably well, as discussed above. This provides support for our further investigation of the atomic-level interactions between halothane and this designed model membrane protein, as well as halothane's modulation of the protein dynamics, as described below.

We have described in an earlier context that halothane exhibits a substantial degree of rotational and translational motion within the cavity, and these appear to be coupled. Namely particular locations and orientations were found to persist for significant durations of time that might suggest the formation and breaking of hydrogen bonds, noting their dynamic nature. Hydrogen-bond formation could potentially occur between halothane and the residues forming or adjacent to the cavity (Fig. 5). On the one hand, it has been found that hydrogen-bond formation can involve the association of

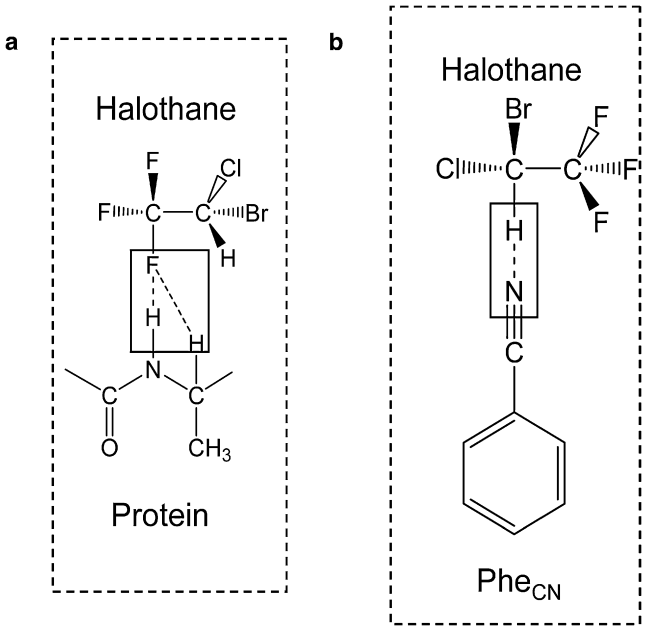

FIGURE 5 Two possibilities were considered for hydrogen-bond formation. (*a*) hydrogen-bond formation between the halothane trifluorine atoms and the backbone hydrogen atoms. (*b*) Hydrogen-bond formation between the acidic hydrogen of the halothane and the nitrile nitrogen of the Phe$_{CN}$ residue.

the halothane trifluorine atoms as the hydrogen-bond acceptor with side chain or backbone hydrogen atoms serving as the donor (28,29). On the other hand, the electronegative nitrogen of the nitrile group can also act as a hydrogen-bond acceptor, thereby the potential for weak hydrogen-bond formation between the acidic hydrogen of halothane and the nitrile nitrogen cannot be precluded.

To explore which of these two types of hydrogen-bond interaction may exist or dominate the stabilization of the halothane within the cavity, we analyzed the correlations between the halothane's rotational motion and the distance of approach of its relevant hydrogen-bond acceptor or donor atoms to the cavity's backbone hydrogen atoms or the Phe$_{CN}$ residues' nitrile-nitrogen atom, respectively.

Halothane's interaction with the backbone hydrogens

Frequent hydrogen bonds appear to form between the trifluorines of halothane and the backbone hydrogens of Ala residues that form the binding cavity (Fig. 6, *b–d*). The association and dissociation of the hydrogen bonds are the result of competition between the four alanine residues, which lie at the same level along the bundle long axis with equal opportunities for approach by the halothane. The orientation of halothane changes in a stepwise manner, each phase strongly correlating with the change of the distance between halothane trifluorines and Ala backbone hydrogens (Fig. 6, *a* and *b–d*). We further explored the instantaneous configurations at different phases of halothane's orientation to match the halothane's motion to its interaction with the cavity, with different phases of orientation denoted as 1–5 as shown in Fig. 6. In phase 1 (0–360 ps), the trifluorines formed hydrogen bonds with the Ala^{139} backbone Cα-hydrogen; in phase 2 (360–560 ps), the halothane flipped its trifluorines toward the Ala^{139} backbone amide-hydrogen; in phase 3 (560–630 ps), the trifluorines formed hydrogen-bonds network with Ala^{99} backbone Cα-hydrogen; in phase 4 (630–700ps), the halothane flipped its

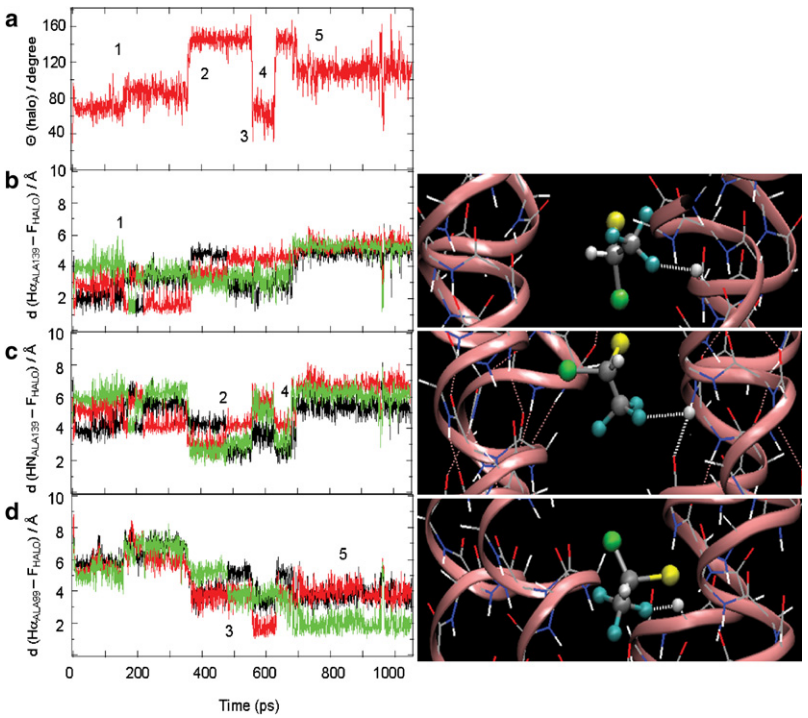

FIGURE 6 Correlations between the halothane's rotational motion (*a*) and the distance of approach of its relevant hydrogen-bond acceptor atoms to the cavity's backbone hydrogen atoms (*b–d*), which is shown in Fig. 5 *a*. (*a*) Halothane's rotational angle θ is defined as in Fig. 3. (*b–d*) The distance between the halothane trifluorines (three fluorines are shown in three different colors) and the adjacent Ala (Ala^{139} in *b* and *c*, Ala^{99} in *d*) backbone amide-H (H$_N$) or C$_\alpha$-H (H$_\alpha$). In *a*, the numbers 1–5 denotes the different phases of the halothane's orientation. Each phase is then matched well to the interaction between the halothane and the cavity backbone hydrogen atoms shown in the right panels of *b–d*. In the right panels, hydrogen bonds between the trifluorines and the H$_N$ or the H$_\alpha$ are represented in white dashed lines. Particularly, in right panel *c*, the same H$_N$ also forms a hydrogen bond with the backbone carbonyl oxygen, which is responsible for stabilizing the protein secondary structure. The peptide is shown in ribbon representation with backbone atoms in wire-frame representation. Nitrogen is colored in blue, oxygen in red, and carbon in silver. The halothane molecule is shown in CPK representation with trifluorines colored in cyan, bromine in yellow, chlorine in green, and hydrogen in white.

trifluorines back toward the Ala^{139} backbone amide-hydrogen, having the same orientation as in phase 2; in phase 5 (700–1100 ps.), trifluorines formed H-bonds with the Ala^{99} Cα-hydrogen (Here Ala^{19}, Ala^{99}, Ala^{139} represent individual Ala residues at position 19 on different helices). The above results demonstrate that halothane's motion inside the cavity is controlled by the interaction of the trifluorine end of halothane with the adjacent Ala backbone hydrogens.

It is also worth noting that, although halothane interacts specifically with backbone hydrogen forming hydrogen bonds, the nature of this bonding is weak and quite dynamic. Examination of the amide hydrogens involved in this specific interaction with halothane shows that those hydrogen bonds responsible for protein secondary structure remain intact. For example, in Fig. 6 *c*, one of the trifluorines of the halothane forms a hydrogen bond with the Ala^{139} amide-hydrogen. However, in the process, the hydrogen bond between the Ala^{139} amide hydrogen (i) and the $Phe_{CN}{}^{135}$ (i-4) carbonyl oxygen remains intact, namely, the distance between this pair of hydrogen-bond donor/acceptor is not perturbed by the hydrogen-bond formation between the same amide H and halothane trifluorines. The weak and dynamic nature of this hydrogen bonding explains why halothane retains substantial translational and rotational motion within the cavity designed into the core bundle.

Halothane's interaction with the vibrational probes

The distance between the acidic hydrogen of the halothane and the nitrile nitrogen of the Phe_{CN} residues is at the large extreme for satisfying a hydrogen-bond distance requirement (Fig. 7 *a*). Furthermore, the stepwise change in the halothane's rotational motion does not correlate with the change of the distance between the halothane hydrogen and the Phe_{CN} nitrile nitrogen (Fig. 7, *a* and *b*). A parallel simulation (simulation II) that samples rather different orientations of halothane also provided similar results (Fig. 7, *c* and *d*).

To further investigate whether a direct interaction between the halothane hydrogen and the Phe_{CN} nitrile-nitrogen might exist, we also removed the partial charges on nitrile groups. Under this circumstance, with the presumed hydrogen-bond acceptor eliminated, we expected an instantaneous change of the halothane's motion, namely the orientation of halothane should change faster and the distance between the halothane hydrogen and the nitrile nitrogen should also become larger. We analyzed two parallel simulations with each of them providing rather different results, but leading to the same conclusion. For simulation I, both the orientation of halothane and the distance between the halothane hydrogen and the nitrile nitrogen remained the same for most of the remainder of the trajectory after removal of the partial charges (Fig. 7, *a* and *b*). For simulation II, over the first 100 ps, three out of four nitrile nitrogens became instantaneously closer to the halothane hydrogen, and the fourth Phe_{CN} nitrogen remained at the same distance from the halothane hydrogen as before the partial charges removed (Fig. 7 *d*). The instantaneous change of the halothane's orientation in this case may be caused by the sudden change of the distance between the halothane hydrogen and the three Phe_{CN} nitrogens (Fig. 7, *c* and *d*). In this case, particular orientations of halothane also persisted even longer than before the partial charge was removed (Fig. 7 *c*). These results contradict the expectations, discounting a direct

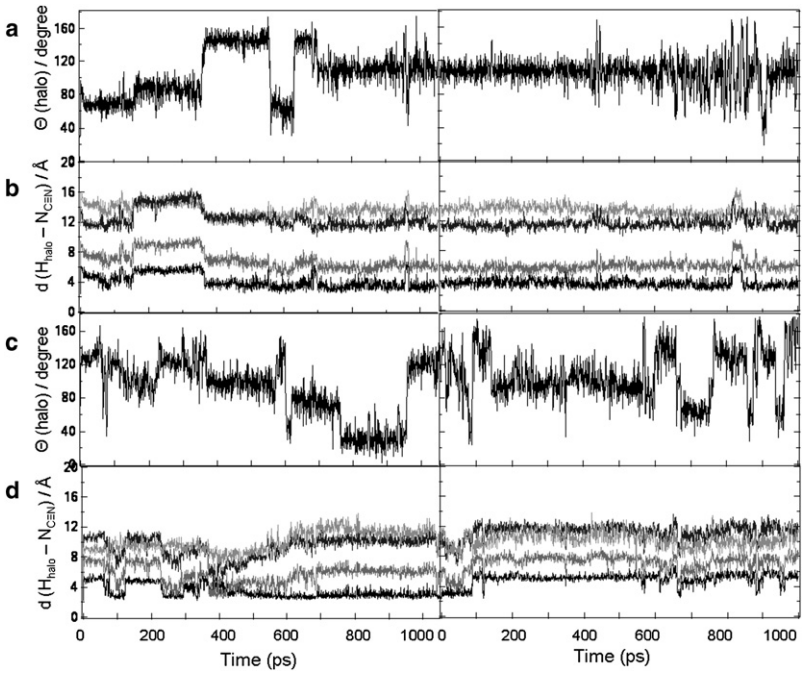

FIGURE 7 For two parallel simulations (simulation I, *a* and *b*; simulation II, *c* and *d*), correlations between the halothane's rotational motion (*a* and *c*) and the distance of approach of its relevant hydrogen-bond donor to the Phe_{CN} residues' nitrile-nitrogen (*b* and *d*), as presented in Fig. 5 *b*, were studied with partial charges on nitrile groups included (*left four panels*) or removed (*right four panels*). (*a* and *c*) The halothane's orientational angle θ is defined as in Fig. 3. (*b* and *d*) The distance between acidic hydrogen of the halothane and the nitrile-nitrogen of the four Phe_{CN} residues are plotted, with each of them in a different gray scale.

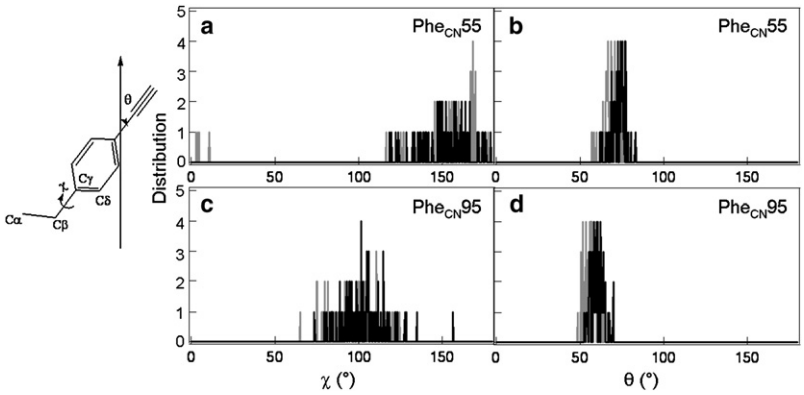

FIGURE 8 Distribution of the aromatic ring's motion for two Phe$_{CN}$ residues in the absence (*gray bar*) and presence of the halothane (*black bar*). χ is defined as the dihedral angle for C_α-C_β-C_γ-C_δ, characterizing the ''flipping'' motion of the aromatic ring; θ is defined as the angle between C_β-C_γ and the bundle long axis, characterizing the ''tilting'' motion of the aromatic ring. The residues in consideration are two Phe$_{CN}$ residues that are closer to the halothane. The addition of halothane seems to have no apparent effect on the widths of the distributions for either of these motions of aromatic rings for either of the two Phe$_{CN}$ residues, indicating the absence of an interaction between halothane and aromatic rings of Phe$_{CN}$ probes.

interaction between the halothane hydrogen and Phe$_{CN}$ nitrile-nitrogen.

Several studies of tryptophan containing halothane-binding model proteins suggest a direct interaction of halothane with tryptophan residues (30,31), reasoning that there is potential for an attractive ''cation-pi'' interaction between the acidic hydrogen of halothane and the highly polarizable indole ring π-electrons (6,7). We did not observe any orientation of the C-H acceptor group of halothane with respect to the sp^2 carbons of the Phe$_{CN}$ aromatic ring residues that would support such an interaction over the entire simulation trajectory. We also examined both the ''flipping'' and the ''tilting'' motions of aromatic ring for the two Phe$_{CN}$ residues that are closer to the halothane. The addition of halothane has no apparent effect on the widths of the distributions for either of these motions of aromatic rings for either of the two Phe$_{CN}$ residues. These results suggest that halothane has no effect on the aromatic rings' dynamics, in turn suggesting the absence of an interaction between halothane and the aromatic rings of the Phe$_{CN}$ probes in our system (see Fig. 8 for details).

Halothane's modulation of protein dynamics

Investigating the effect of anesthetics on protein dynamics is important because protein function can necessarily involve internal protein motion(s). By investigating halothane's modulation of protein dynamics, we may obtain valuable information that would guide further development of such anesthetic-binding model membrane proteins, but also may rationalize how anesthetics might modulate membrane protein function.

Fig. 9 shows the root mean square deviation (RMSD) of backbone Cα atoms of the hbAP1-Phe$_{CN}$ 4-helix bundle with respect to the equilibrated structure summed over all residues as a function of time. We calculated this RMSD for hbAP1-Phe$_{CN}$ in the absence and presence of halothane. There is no apparent difference between these two trajectories, suggesting that the introduction of halothane has no effect on the overall backbone structure of the protein. This result further indicates that the associated quaternary structure of the 4-helix bundle is also stable to the introduction of halothane.

The more profound effects of halothane were discovered in the protein dynamics. The root mean square fluctuation (RMSF) of backbone C atoms for each residue of the hbAP1-Phe$_{CN}$ was computed in the absence and presence of halothane, as shown in Fig. 10. The backbone dynamics of both forms (with or without halothane) exhibit a greater flexibility than those of natural ion channel proteins (29,32). The terminal and Gly linker-loop residues appear to be most flexible, not surprisingly. The most profound changes are seen in the overall decrease of RMSF upon binding the halothane, although it is more apparent in the case of helix H3 and H4. (We found that in this simulation, the halothane is ~2–4 Å closer to helices H3 and H4 compared to helices H1 and H2 during the trajectory. On the timescale of these simulations, the halothane molecule

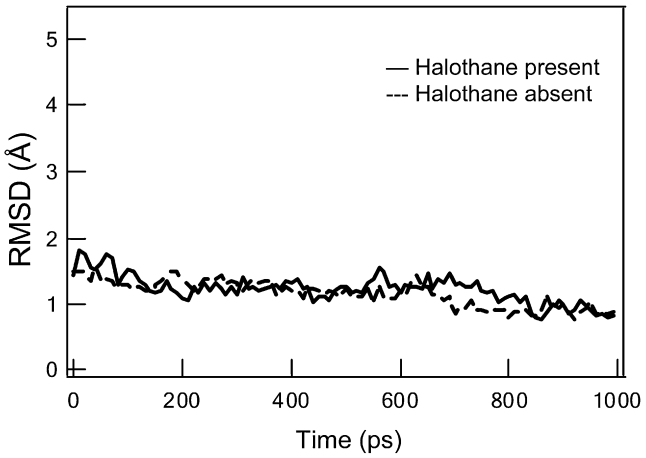

FIGURE 9 Halothane's impact on the backbone structure of the hbAP1-Phe$_{CN}$ peptide bundle. Shown here is a comparison of the computed RMSD of backbone C_α atoms in the absence (*dashed line*) and presence (*solid line*) of the halothane molecule, respectively. The equation for calculating RMSD is as follows: $\mathrm{RMSD} = \left[\frac{1}{M}\sum_{i=1}^{M}(R_i - R_i^{\mathrm{eq}})^2\right]^{1/2}$, where R_i and R_i^{eq} are the coordinates of the ith backbone C_α of an instantaneous structure and the equilibrated structure, respectively.

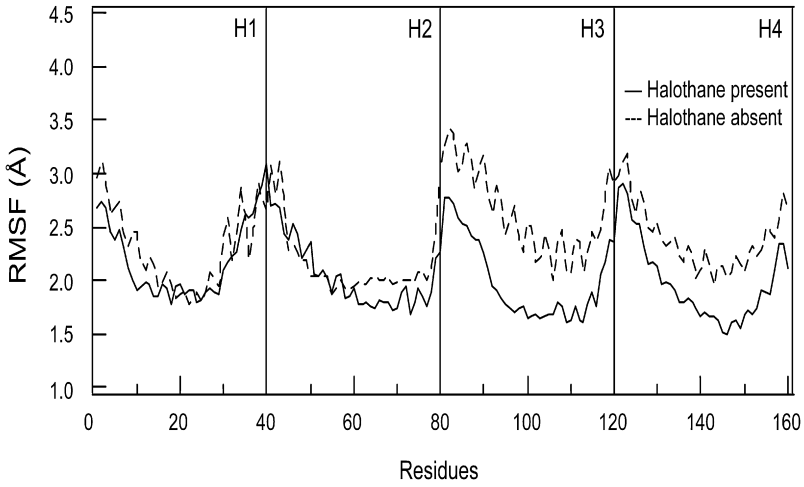

FIGURE 10 Comparison of the backbone dynamics of the hbAP1-Phe$_{CN}$ peptide bundle in the absence (*dashed line*) and presence (*solid line*) of halothane. Shown here is the computed RMSF of backbone C_α atoms for each residue. The four helices in the bundle are named H1, H2, H3, and H4. H1 and H2 are within one dimer; H3 and H4 belong to the other dimer. The equation for calculating RMSF is as follows: $\mathrm{RMSF} = \left[\frac{1}{T}\sum_{tj=1}^{T}(R_{i(tj)} - \overline{R_i})^2\right]^{1/2}$, where $R_{i(tj)}$ and $\overline{R_i}$ are the coordinates of the ith backbone C_α of an instantaneous structure at time tj and the coordinates averaged over time T, respectively. Note that the difference between RMSD and RMSF is that with the later the average is taken over time T, giving a value for each residue i; with RMSD the average is taken over the M residues, giving time specific values.

moves initially from a central position within the cavity of the peptide bundle to become associated with one of the two pairs of helices, and remains so-associated for the remainder of the trajectory. However, this phenomena is random, namely the halothane can become associated with a different pair of helices in a parallel simulation.) In the presence of halothane, there seems to be slightly larger suppression of the backbone's motion in the vicinity of the halothane binding cavity than at the ends of the bundle upon the introduction of halothane. In any case, the overall trend is quite clear—the binding of halothane reduces the global dynamics of protein backbone. This result agrees with the implications from NMR findings of a water-soluble halothane-binding 4-helix bundle peptide (31,33), namely that halothane stabilizes overall protein motion.

CONCLUSIONS

We have investigated the use of Phe$_{CN}$ as a spectroscopic probe of the local environment in the neighborhood of a designed halothane-binding cavity within a model membrane protein by classical MD simulations. To our knowledge, this is the first time an infrared probe and MD simulations have been used to study anesthetic binding to model membrane proteins. The blue-shift in the nitrile vibrational frequency upon binding halothane predicted by MD simulations is in good agreement with the infrared experiments. We demonstrated the absence of any direct interaction between halothane and the nitrile groups, indicating a minimal perturbation by the introduction of Phe$_{CN}$ to investigate the interaction of halothane with the cavity, making it an ideal ''spectator'' probe of local environment inside the protein. The frequency shift is largely ascribed to the change in the probes' electrostatic protein environment induced by the halothane rather than the change of solvent accessibility of infrared probes. The backbone structure of the apo peptide bundle appears to be highly flexible. Upon binding the halothane to the cavity, the backbone's motion is significantly quenched with a slightly larger suppression at the vicinity of the halothane binding site, which may contribute to decreasing the dissociation of halothane from the binding site once bound. During the simulation trajectories, halothane remained localized within the hydrophobic cavity within the core of the peptide bundle, while nevertheless exhibiting a substantial degree of translational and rotational motions. Although interaction between halothane and the cavity's backbone hydrogens dominates, the nature of this interaction is still weak and quite dynamic and does not compete with hydrogen bonds responsible for protein's secondary structure. The weakness of this interaction explains why the halothane retains substantial motion while localized within the cavity. Collectively, the rich information displayed from simulations could provide significant insight into the interaction between anesthetic molecules and membrane proteins. Further improvements could target labeling the cavity residues (i.e., alanine) directly.

SUPPORTING MATERIAL

A table, a figure, and Note S1 are available at http://www.biophysj.org/biophysj/supplemental/S0006-3495(09)00609-2.

The authors greatly appreciate the computer time on clusters of the Nanoscale Biomoleclar Materials under Liniac project at the University of Pennsylvania and Chemistry Computer Facility at the University of Pennsylvania.

This research is supported primarily by the National Institutes of Health grant P01-GM55876. J.K.B. and H.Z. acknowledge the support from the National Science Foundation's Materials Research Science and Engineering Center program DMR05-20020.

REFERENCES

1. Johansson, J. S. 2003. Noninactivating tandem pore domain potassium channels as attractive targets for general anesthetics. *Anesth. Analg.* 96:1248–1250.
2. Chiara, D. C., L. J. Dangott, R. G. Eckenhoff, and J. B. Cohen. 2003. Identification of nicotinic acetylcholine receptor amino acids photolabeled by the volatile anesthetic halothane. *Biochemistry.* 42:13457–13467.

3. Ye, S. X., J. Strzalka, I. Y. Churbanova, S. Y. Zheng, J. S. Johansson, et al. 2004. A model membrane protein for binding volatile anesthetics. *Biophys. J.* 87:4065–4074.

4. Churbanova, I. Y., A. Tronin, J. Strzalka, T. Gog, I. Kuzmenko, et al. 2006. Monolayers of a model anesthetic-binding membrane protein: Formation, characterization, and halothane-binding affinity. *Biophys. J.* 90:3255–3266.

5. Strzalka, J., J. Liu, A. Tronin, J. S. Johansson, and J. K. Blasie. 2009. Mechanism of interaction between the general anesthetic halothane and a synthetic protein model ion channel, I: structural investigations via x-ray reflectivity from Langmuir monolayers. *Biophys. J.* 96:4164–4175.

6. Johansson, J. S., B. R. Gibney, F. Rabanal, K. S. Reddy, and P. L. Dutton. 1998. A designed cavity in the hydrophobic core of a four-alpha-helix bundle improves volatile anesthetic binding affinity. *Biochemistry.* 37:1421–1429.

7. Katz, B. A., B. S. Liu, and R. Cass. 1996. Structure-based design tools: structural and thermodynamic comparison with biotin of a small molecule that binds to streptavidin with micromolar affinity. *J. Am. Chem. Soc.* 118:7914–7920.

8. Getahun, Z., C. Y. Huang, T. Wang, B. De Leon, W. F. DeGrado, et al. 2003. Using nitrile-derivatized amino acids as infrared probes of local environment. *J. Am. Chem. Soc.* 125:405–411.

9. Yoshikawa, S., D. H. Okeeffe, and W. S. Caughey. 1985. Investigations of cyanide as an infrared probe of hemeprotein ligand-binding sites. *J. Biol. Chem.* 260:3518–3528.

10. Liu, J., J. Strzalka, A. Tronin, J. S. Johansson, and J. K. Blasie. 2009. Mechanism of interaction between the general anesthetic halothane and a model ion channel protein, II: fluorescence and vibrational spectroscopy using a cyanophenylalanine probe. *Biophys. J.* 96:4176–4187.

11. Tuckerman, M. E., and G. J. Martyna. 2000. Understanding modern molecular dynamics: techniques and applications. *J. Phys. Chem. B.* 104:159–178.

12. Hansson, T., C. Oostenbrink, and W. F. van Gunsteren. 2002. Molecular dynamics simulations. *Curr. Opin. Struct. Biol.* 12:190–196.

13. Roux, B., and K. Schulten. 2004. Computational studies of membrane channels. *Structure.* 12:1343–1351.

14. Adcock, S. A., and J. A. McCammon. 2006. Molecular dynamics: survey of methods for simulating the activity of proteins. *Chem. Rev.* 106:1589–1615.

15. Kale, L., R. Skeel, M. Bhandarkar, R. Brunner, A. Gursoy, et al. 1999. NAMD2: greater scalability for parallel molecular dynamics. *J. Comput. Phys.* 151:283–312.

16. MacKerell, A. D., D. Bashford, M. Bellott, R. L. Dunbrack, J. D. Evanseck, et al. 1998. All-atom empirical potential for molecular modeling and dynamics studies of proteins. *J. Phys. Chem. B.* 102:3586–3616.

17. Jorgensen, W. L., J. Chandrasekhar, J. D. Madura, R. W. Impey, and M. L. Klein. 1983. Comparison of simple potential functions for simulating liquid water. *J. Chem. Phys.* 79:926–935.

18. Yin, D. 1997. Parameterization for empirical force field calculations and a theoretical study of membrane permeability of pyridine derivative. PhD thesis. Department of Pharmaceutical Sciences. University of Maryland, College Park, MD.

19. Liu, Z. W., Y. Xu, A. C. Saladino, T. Wymore, and P. Tang. 2004. Parametrization of 2-bromo-2-chloro-1,1,1-trifluoroethane (halothane) and hexafluoroethane for nonbonded interactions. *J. Phys. Chem. A.* 108:781–786.

20. Zou, H. L., J. Strzalka, T. Xu, A. Tronin, and J. K. Blasie. 2007. Three-dimensional structure and dynamics of a de novo designed, amphiphilic, metallo-porphyrin-binding protein maquette at soft interfaces by molecular dynamics simulations. *J. Phys. Chem. B.* 111:1823–1833.

21. Rey, R., and J. T. Hynes. 1998. Vibrational phase and energy relaxation of CN- in water. *J. Chem. Phys.* 108:142–153.

22. Hutchinson, E. J., and D. Ben-Amotz. 1998. Molecular force measurement in liquids and solids using vibrational spectroscopy. *J. Phys. Chem. B.* 102:3354–3362.

23. Suydam, I. T., C. D. Snow, V. S. Pande, and S. G. Boxer. 2006. Electric fields at the active site of an enzyme: Direct comparison of experiment with theory. *Science.* 313:200–204.

24. Andrews, S. S., and S. G. Boxer. 2002. Vibrational Stark effects of nitriles II. Physical origins of stark effects from experiment and perturbation models. *J. Phys. Chem. A.* 106:469–477.

25. Andrews, S. S., and S. G. Boxer. 2000. Vibrational stark effects of nitriles I. Methods and experimental results. *J. Phys. Chem. A.* 104:11853–11863.

26. Mukherjee, S., P. Chowdhury, W. F. DeGrado, and F. Gai. 2007. Site-specific hydration status of an amphipathic peptide in AOT reverse micelles. *Langmuir.* 23:11174–11179.

27. Zou, H. L., M. J. Therien, and J. K. Blasie. 2008. Structure and dynamics of an extended conjugated NLO chromophore within an amphiphilic 4-helix bundle peptide by molecular dynamics simulation. *J. Phys. Chem. B.* 112:1350–1357.

28. Dipaolo, T., and C. Sandorfy. 1974. Hydrogen-bond breaking potency of fluorocarbon anesthetics. *J. Med. Chem.* 17:809–814.

29. Tang, P., and Y. Xu. 2002. Large-scale molecular dynamics simulations of general anesthetic effects on the ion channel in the fully hydrated membrane: The implication of molecular mechanisms of general anesthesia. *Proc. Natl. Acad. Sci. USA.* 99:16035–16040.

30. Davies, L. A., M. L. Klein, and D. Scharf. 1999. Molecular dynamics simulation of a synthetic four-alpha-helix bundle that binds the anesthetic halothane. *FEBS Lett.* 455:332–338.

31. Cui, T. X., V. Bondarenko, D. J. Ma, C. Canlas, N. R. Brandon, et al. 2008. Four-alpha-helix bundle with designed anesthetic binding pockets. Part II: halothane effects on structure and dynamics. *Biophys. J.* 94:4464–4472.

32. Domene, C., S. Vemparala, S. Furini, K. Sharp, and M. L. Klein. 2008. The role of conformation in ion permeation in a K+ channel. *J. Am. Chem. Soc.* 130:3389–3398.

33. Ma, D. J., N. R. Brandon, T. X. Cui, V. Bondarenko, C. Canlas, et al. 2008. Four-alpha-helix bundle with designed anesthetic binding pockets; Part I: structural and dynamical analyses. *Biophys. J.* 94:4454–4463.